# Rules for controlling low-dimensional vocal fold models with muscle activation

Ingo R. Titze[a)]
*National Center of Voice and Speech, and Department of Speech Pathology and Audiology, The University of Iowa, Iowa City, Iowa 52242 and the Wilbur James Gould Voice Research Center, Denver Center for the Performing Arts, Denver, Colorado 80204*

Brad H. Story
*Department of Speech and Hearing Sciences, University of Arizona, Tuscon, Arizona 85721*

(Received 18 June 1998; revised 3 May 2002; accepted 31 May 2002)

A low-dimensional, self-oscillation model of the vocal folds is used to capture three primary modes of vibration, a shear mode and two compressional modes. The shear mode is implemented with either two vertical masses or a rotating plate, and the compressional modes are implemented with an additional bar mass between the vertically stacked masses and the lateral boundary. The combination of these elements allows for the anatomically important body-cover differentiation of vocal fold tissues. It also allows for reconciliation of lumped-element mechanics with continuum mechanics, but in this reconciliation the oscillation region is restricted to a nearly rectangular glottis (as in all low-dimensional models) and a small effective thickness of vibration ($<3$ mm). The model is controlled by normalized activation levels of the cricothyroid (CT), thyroarytenoid (TA), lateral cricoarytenoid (LCA), and posterior cricoarytenoid (PCA) muscles, and lung pressure. An empirically derived set of rules converts these muscle activities into physical quantities such as vocal fold strain, adduction, glottal convergence, mass, thickness, depth, and stiffness. Results show that oscillation regions in muscle activation control spaces are similar to those measured by other investigations on human subjects. 
[DOI: 10.1121/1.1496080]

PACS numbers: 43.70.Bk [AL]

## I. INTRODUCTION

This paper addresses an ongoing search for a link between laryngeal muscle activation and mechanical properties of simple mass-spring vocal fold models. Although finite element implementation of continuum models of the vocal folds (Alipour and Titze, 1983, 1996), the tongue (Wilhelms-Tricarico, 1995), and the velum (Berry *et al.*, 1999) offer the potential for embedding muscle contractions directly into the mathematical formulations, the appeal of simple lumped-element models of tissue remains. This is partly due to the conceptual simplicity of coupled masses and springs, and partly due to the interpretive power that nonlinear dynamics has to offer to low-dimensional models (two or three degrees of freedom).

Low-dimensional models of the vocal folds have traditionally been structured to capture two or three primary modes of tissue vibration, one shear mode and one or two compressional modes (for identification and nomenclature of a complete set of modes, see Titze and Strong, 1975; Berry and Titze, 1996). In a continuum model, the compressional modes do not truly represent tissue compression, because human tissues are incompressible at audio frequencies, but there is an *apparent* compression in the horizontal direction while there is an *apparent* expansion in the vertical direction, leaving the volume conserved. In fact, all vocal fold deformations involve shear (Titze and Talkin, 1979). The one-mass model of Flanagan and Landgraf (1968) captured only one compressional mode, the two-mass model of Ishizaka and Flanagan (1972) captured both a shear mode and a compressional mode, but not in an explicit body-cover manner. The translational-rotational model of Liljencrants (1991) was designed expressly to control the shear mode independently from the compressional mode, but the body-cover distinction was still not clear. The three-mass model of Story and Titze (1995) captured three modes, one shear mode and two compressional modes, with the extra degree of freedom allowing a body-cover differentiation. Thus, if low-dimensionality, mode separation, and body-cover differentiation are all of primary interest, the translational-rotational model of Liljencrants (with minor modifications) or the three-mass model of Story and Titze are logical choices.

The problem is that vocal fold parameters such as normal mode frequencies, stiffness, effective mass in vibration, vocal fold length, vocal fold thickness, and rest position may not be under direct control by the vocalist. Rather, perceptual dimensions such as loudness, pitch, register, tightness, and roughness are likely to govern the thought processes for activation of laryngeal and respiratory muscles. Thus, to understand the oscillatory characteristics of the vocal folds in perceptual and physiologically realistic control spaces, we need one set of rules that transform perceptual variables to muscle activations, and a second set of rules that transform muscle activations to geometrical and viscoelastic parameters of the

a)Electronic mail: ingo-titze@uiowa.edu

 

lumped element models. We address only the second set of rules here.

It must be stated at the outset that no physiologically realistic vocal fold model is simple. If simplicity is forced onto the mechanics of the model, then the rules for control are complicated, as will be seen in this paper. On the contrary, less complicated rules are needed for models that incorporate the three-dimensional (continuum) nature of vocal fold mechanics, but at the price of greater mathematical complexity.

## II. A MINIMAL PARAMETER SET

As a minimum, the following parameters are needed to capture the lowest natural modes and to relate the lumped-element mechanics of the tissue layers to the distributed surface pressures in the glottis:

(1) A compressional stiffness ($K$) for the body of the vocal folds and a rotational shear stiffness ($\kappa$) for the cover to control the natural frequencies of oscillation (and less directly, the fundamental frequency $F_o$). These two stiffnesses can be related to two independent elastic constants of an elastic continuum, a Poisson ratio and a shear modulus.
(2) The length ($L$), thickness ($T$), and depth ($D$) of the vocal folds to define boundary constraints and the vocal fold dimensions.
(3) The depth of the cover ($D_c$) to separate the body tissue layer from the cover tissue layer in terms of effective mass of vibration.
(4) The glottal half-width ($\xi_{02}$) at the top of the vocal fold to control the adduction of the vocal processes.
(5) The net glottal convergence ($\xi_c$) from the bottom of the vocal folds to the top of the vocal folds to control medial surface geometry.
(6) The mucosal upheaval point along the medial surface of the vocal folds or, correspondingly, the nodal point ($z_n$) of the shear mode to control upper and lower amplitudes of vibration.

With the use of these parameters, we first begin to review the mechanics of vocal fold vibration as applied to a three degrees of freedom body-cover model. Muscle activation will be brought into the picture later by rules.

## III. LOW-DIMENSIONAL BODY-COVER MODELS

We begin the quantification of self-sustained oscillation with a body-cover model that has only three degrees of freedom. As illustrated in Fig. 1 in coronal cross-section, the cover is represented by either two masses $m_1$ and $m_2$ and three springs $k_1$, $k_2$, and $k_c$ (left side) or by a rotating plate of mass $m$ with a torsional stiffness $\kappa$ and a single spring $k$ (right side). The body is represented by a mass $M$ in both cases, connected through a compressible spring $K$ to the thyroid cartilage boundary. We shall refer to these two models as the *three mass* and the *bar-plate* version of the body-cover model, respectively. The models have no variation perpendicular to the plane of the paper (the anterior-posterior direction, or $y$ direction), which means that the masses are rigid rods, plates, or bars. In the bar-plate model, the cover spring $k$ attaches at the point of rotation (nodal point $z_n$) of the plate, which is not necessarily at the center of the bar. The $z$ direction is the direction of airflow and the $x$ direction is the direction of medial-lateral tissue displacement.

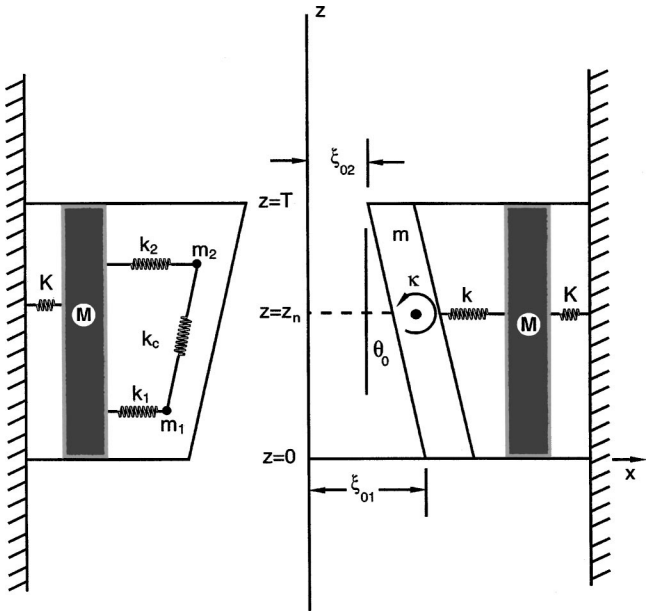


FIG. 1. Sketch of three-mass (left) and bar-plate (right) low-dimensional body-cover models in frontal cross section.

Unless otherwise stated, we make the following assumptions throughout the body-cover derivations: (1) The two vocal folds move symmetrically with respect to the glottal midplane ($x=0$). (2) There is no vertical displacement of tissue. (3) The nodal point $z_n$ can move vertically, redistributing the mass in the cover. (4) The glottal area varies linearly from the bottom to top of the vocal folds.

The equations for glottal aerodynamics of this model have already been published (Titze, 2002) and will not be repeated here. Briefly, we assume Bernoulli flow from the lungs to the point of flow separation, at which point jet flow continues and the pressure remains constant in the jet, from flow detachment to glottal exit. Liljencrants' (1991) rules or those of Pelorson *et al.* (1994) for a slightly enlarged detachment area and a downstream detachment point have been incorporated. Furthermore, for this investigation, we have not included any vocal tract simulation. We realize that vocal fold vibration can be profoundly affected by the acoustic load of the vocal tract, but this will be treated in a follow-up investigation and does not impact on the rules developed here.

### A. Equations of motion for three degrees of freedom

Consider first the motion of the vocal fold cover in the bar-plate version (right side of Fig. 1). This motion can be described with two degrees of freedom if we assume a rotation $\theta$ about the nodal point $z_n$ and a translation $\xi$ of the nodal point,

$$I_c\ddot{\theta}+B_c\dot{\theta}+\kappa\theta=T_a, \tag{1}$$

$$m\ddot{\xi}+b(\dot{\xi}-\dot{\xi}_b)+k(\xi-\xi_b)=F_a, \tag{2}$$

where $T_a$ is the applied aerodynamic torque, $I_c$ is the moment of inertia for rotation of the cover, $B_c$ is the rotational damping, $b$ is translational damping, $F_a$ is the force at the nodal point, $\xi_b$ is the displacement of the body, and other parameters are as previously defined. Similarly, the equation of motion for the body is written as

$$M\ddot{\xi}_b + b(\dot{\xi}_b - \dot{\xi}) + k(\xi_b - \xi) + K\xi_b + B\dot{\xi}_b = 0, \tag{3}$$

where $B$ is the body damping.

The natural frequencies of this body-cover system can be obtained analytically by letting all damping forces and aerodynamic forces vanish (i.e., $b=B=B_c=T_a=F_a=0$) and assuming harmonic functions of the form $e^{i\omega t}$. The result is

$$\omega_2^2 = \kappa/I_c \tag{4}$$

for the shear mode, and

$$\omega_{1,3}^2 = \frac{k+K}{2M} + \frac{k}{2m} \pm \left[ \left( \frac{k+K}{2M} + \frac{k}{2m} \right)^2 - \frac{kK}{mM} \right]^{1/2} \tag{5}$$

for the two compressional modes. As an asymptotic check, the compressional mode frequencies in Eq. (5) reduce to

$$\omega_{1,3}^2 = \frac{k}{m} \quad \text{for } M \gg m \tag{6}$$

$$= \frac{K}{M+m} \quad \text{for } k \gg K \tag{7}$$

$$= k\frac{M+m}{Mm} \quad \text{for } K=0 \tag{8}$$

$$= 0 \quad \text{for } k=0 \text{ or } m=\infty. \tag{9}$$

When the driving forces are not zero, Eqs. (1) and (2) are coupled by the fact that both the driving torque $T_a$ and the driving force $F_a$ on the cover are dependent on a common glottal flow.

The equations of motion for the three-mass model (left side of Fig. 1) are described in detail by Story and Titze (1995). We add only a variable mass distribution in the cover by letting $m_1$ and $m_2$ depend on the nodal point $z_n$,

$$m_1 = mz_n/T, \tag{10}$$

$$m_2 = m(1 - z_n/T), \tag{11}$$

$$k_1 = kz_n/T, \tag{12}$$

$$k_2 = k(1 - z_n/T), \tag{13}$$

where $m$ and $k$ are the bar-plate constants as defined above.

The relation between the vertical coupling stiffness $k_c$ in the three-mass model and the rotational stiffness $\kappa$ in the bar-plate model can be found by equating $\omega_2$ (the normal mode frequency for shear) of the two models when the body mass $M$ is rigid. This frequency is defined by Eq. (4) for the bar-plate model, but for the three-mass model a separate modal analysis is performed for the cover, with only the masses $m_1$ and $m_2$, and three springs $k_1$, $k_2$ and $k_c$. The result yields the following equivalence,

$$\omega_2^2 = \frac{\kappa}{I_c} = \frac{k_1+k_c}{2m_1} + \frac{k_2+k_c}{2m_2} + \left[ \left( \frac{k_1+k_c}{2m_1} - \frac{k_2+k_c}{2m_2} \right)^2 + \frac{k_c^2}{m_1 m_2} \right]^{1/2}. \tag{14}$$

Substituting Eqs. (10)–(13) into Eq. (14) gives a relation for $\kappa$ in terms of $k_c$,

$$\kappa = \frac{I_c}{m} \left[ k + k_c \left( \frac{z_n}{T} \right)^{-1} \left( 1 - \frac{z_n}{T} \right)^{-1} \right], \tag{15}$$

and its inverse

$$k_c = \left( \frac{m}{I_c}\kappa - k \right) \left( \frac{z_n}{T} \right) \left( 1 - \frac{z_n}{T} \right). \tag{16}$$

We see that $k_c$ in the three-mass model is a mixture of both shear ($\kappa$) and compression ($k$). This is because one of the three springs for a two-mass cover is essentially redundant.

When there is symmetry between the upper and lower mass, then

$$m_1 = m_2 = m/2, \tag{17}$$

$$k_1 = k_2 = k/2, \tag{18}$$

and the vertical coupling stiffness is related to the torsional stiffness as

$$k_c = \frac{1}{4} \left( \frac{m}{I_c}\kappa - k \right). \tag{19}$$

Equations (16) and (19) show that there are some restrictions on the choices of $\kappa$ and $k$ if the coupling stiffness $k_c$ is to be a positive number. We will now explore these restrictions on the basis of continuum mechanics.

### B. Relating lumped constants to elastic moduli

The purpose of adopting continuum-mechanical constants for modeling is that they are independent of geometry and, therefore, become the basic building blocks for both distributed and lumped element representations. For a negligible amount of fiber tension in the vocal folds, it is possible to express the translational and rotational stiffnesses in terms of one measurable isotropic shear modulus (Chan and Titze, 1997). Referring to continuum mechanics, the constitutive equations for transversely isotropic tissue with planar strain (Fung, 1993) can be written as

$$\sigma_x = \frac{2\mu}{(1-\nu)} \left( \frac{\partial \xi}{\partial x} + \nu \frac{\partial \zeta}{\partial z} \right) \tag{20}$$

and

$$\tau_{xz} = \mu \left( \frac{\partial \xi}{\partial z} + \frac{\partial \zeta}{\partial x} \right), \tag{21}$$

where $\sigma_x$ is the normal stress in the $x$ direction, $\tau_{xz}$ is the shear stress on a $z$ plane in the $x$ direction, $\mu$ is the shear modulus, $\nu$ is the Poisson ratio, $\xi$ is horizontal displacement, and $\xi$ is vertical displacement. The two independent elastic constants are $\mu$ and $\nu$, but since we have already assumed $\zeta=0$ to reduce the number of degrees of freedom of the model, the tissue must now be treated as completely com-

pressible ($\nu=0$), leaving $\mu$ as the only elastic constant.

If we further assume that all the compression takes place linearly over a depth $D$, then the normal stress is

$$\sigma_x = 2\mu \frac{\partial \xi}{\partial x} = 2\mu \xi / D, \tag{22}$$

and the shear stress is

$$\tau_{xz} = \mu \frac{\partial \xi}{\partial z} = \mu \tan\theta \approx \mu\theta, \tag{23}$$

where $\theta$ is the torsional angle defined in Eq. (1), which is typically assumed to be small in linear elasticity theory.

The normal stress $\sigma_x$ in Eq. (22) can be converted to a net restoring force by multiplying this stress by the cross sectional area of the tissue $LT$,

$$F_x = LT\sigma_x = k\xi. \tag{24}$$

When $\sigma_x$ from Eq. (22) is now substituted into Eq. (24), the spring constant $k$ in the cover becomes

$$k = 2\mu_c LT/D_c, \tag{25}$$

where $\mu_c$ is the shear modulus in the cover and $D_c$ is the depth of the cover. For the body, we can similarly write

$$K = 2\mu_b LT/D_b, \tag{26}$$

where $\mu_b$ is the shear modulus of the body and $D_b$ is the depth of the body. The constants $k_1$ and $k_2$ for the three-mass model are obtained by direct substitution of the above into Eqs. (12) and (13).

For the shear stress in the cover, $\tau_{xz}$ is multiplied by the horizontal shear area $LD_c$ to get a shear restoring force

$$F_\theta = LD_c\mu_c\theta. \tag{27}$$

This shear force is then multiplied by an upper moment arm $(T-z_n)/2$ and a lower moment arm $z_n/2$ to get a restoring torque,

$$T_\theta = (LD_c\mu_c\theta)\left[\frac{T-z_n}{2} + \frac{z_n}{2}\right] = (LD_c\mu_c\theta)\frac{T}{2}. \tag{28}$$

This torque is divided by the angular strain $\theta$ to get the torsional stiffness:

$$\kappa = \tfrac{1}{2}\mu_c LTD_c. \tag{29}$$

Note that the lumped-element spring constants $k$, $K$, and $\kappa$ are all directly proportional to the shear modulus of the tissue, but these spring constants also contain the geometrical factors length, thickness, and depth of the tissue layers. In particular, all stiffnesses increase linearly with vocal fold length and thickness, but rotational stiffness increases with tissue depth [Eq. (29)], whereas compressional stiffnesses decrease with tissue depth [Eqs. (25) and (26)]. Thus, tissue depths are critical for modeling when lumped-element parameters are used.

The effective masses of the body and cover are related to the tissue density $\rho$ and the volume of tissue in vibration,

$$m = \rho LTD_c, \tag{30}$$

$$M = \rho LTD_b. \tag{31}$$

The moment of inertia $I_c$ of the cover can also be derived from basic principles as

$$I_c = \int_0^{z_n} (z_n - z)^2\, dm + \int_{z_n}^{T} (z - z_n)^2\, dm \tag{32}$$

$$= \rho LD_c \int_0^T (z - z_n)^2\, dz \tag{33}$$

$$= \rho LD_c T^3 \left[\frac{1}{3} - \frac{z_n}{T}\left(1 - \frac{z_n}{T}\right)\right]. \tag{34}$$

With these derivations, the natural frequencies of the bar-plate model [Eqs. (4) and (5)] can be calculated analytically in terms of the elastic constants $\mu_c$ and $\mu_b$, the tissue density $\rho$, and vocal fold geometry,

$$F_2 = \frac{1}{2\pi}\sqrt{\frac{\kappa}{I_c}} = \frac{1}{\pi T}\sqrt{\frac{3\mu_c}{4\rho}}\left[\frac{1}{3} - \frac{z_n}{T}\left(1 - \frac{z_n}{T}\right)\right]^{-1/2}, \tag{35}$$

$$F_{1,3} = \frac{1}{2\pi\sqrt{\rho}}\left\{\frac{\mu_c}{D_c^2} + \frac{\mu_c}{D_cD_b} + \frac{\mu_b}{D_b^2} \pm \left[\left(\frac{\mu_c}{D_c^2} + \frac{\mu_c}{D_cD_b} + \frac{\mu_b}{D_b^2}\right)^2 - \frac{4\mu_c\mu_b}{D_b^2D_c^2}\right]^{1/2}\right\}^{1/2}. \tag{36}$$

Note that the nodal point $z_n$ and the vocal fold thickness $T$ affect only the shear mode frequency $F_2$, whereas tissue depths $D_c$ and $D_b$ affect only the two compressional mode frequencies $F_1$ and $F_3$. This makes it easy for the user to adjust the normal modes with geometric factors.

Analytical calculation of the natural frequencies of the three-mass model is also possible, but involves cube-root terms that are mathematically quite cumbersome and take up excessive space.

Note that all three natural frequencies in Eqs. (35) and (36) are proportional to the square root of a ratio between a shear modulus and the tissue density, e.g., $(\mu_c/\rho)^{1/2}$, which dimensionally is a tissue wave velocity. The shear moduli $\mu_c$ and $\mu_b$ have been measured in the laboratory (Chan and Titze, 1997, 1999). For excised cover tissue $\mu_c \approx 500$ Pa and for excised thyroarytenoid muscle tissue, $\mu_b \approx 1000$ Pa, but these moduli can vary significantly depending on moisture content, temperature, and frequency. The density is less variable, $\rho = 1040$ kg/m$^3$, giving a tissue wave velocity $(\mu/\rho)^{1/2}$ in the range of 0.7–1.0 m/s, which agrees with measurement of the mucosal wave (Baer, 1975; Titze *et al.*, 1993).

Equation (16) gave a relation between the vertical coupling spring constant $k_c$ of the three-mass model and the parameters of the bar-plate model. Substituting into Eq. (16) the mass of the cover $m$ from Eq. (30), the moment of inertia $I_c$ from Eq. (34), the torsional spring constant $\kappa$ from Eq. (29), and the stiffness $k$ from Eq. (25), the following inequality must hold for $k_c$ to be a positive number,

$$D_c > 2T\left[\frac{1}{3} - \frac{z_n}{T}\left(1 - \frac{z_n}{T}\right)\right]^{1/2}. \tag{37}$$

As an example, this inequality simplifies to $D_c > 0.577T$ for $z_n/T = 0.5$, a fairly stringent requirement for the depth-to-thickness-ratio of the cover. It points out one of the limitations of the low-dimensional models in achieving a reconcili-

ation with continuum mechanics. As the nodal point shifts up and down, with $z_n/T$ approaching 0 or 1, the restriction becomes even greater. The problem is that a solid bar mass $M$ was chosen for the body. No shear can take place in this element, making the shear depth for the cover effectively too thin. Our rules will pay attention to this problem by limiting vocal fold thickness.

### C. Inclusion of fiber stress in tissues

The foregoing equivalence between continuum mechanics and lumped-element mechanics applies only to the case where there is tissue isotropy, i.e., where there is a negligible anterior–posterior tension in the tissue fibers (muscle and ligament). But the spring constants can be augmented to account for anisotropic (stringlike) tension in the fibers by equating the natural frequency of a mass-spring mode of vibration to an ideal string mode of vibration,

$$\frac{1}{2\pi}\sqrt{\frac{K'}{M}}=\frac{1}{2L}\sqrt{\frac{\sigma}{\rho}}, \tag{38}$$

where $\sigma$ is the fiber stress and $K'$ is the added fiber stiffness. Solving for $K'$ and letting $M=\rho LTD$, the added stiffness is

$$K'=\left(\frac{\pi}{L}\right)^2\sigma LTD=\pi^2\sigma DT/L. \tag{39}$$

For rotational movement, $K'$ is replaced by $\kappa'$ and $M$ is replaced by $I_c$ in the above. The augmented lumped-element parameters now become the following:

*Bar-plate model (cover):*

$$\kappa=\frac{1}{2}\mu_c LTD_c+\pi^2\sigma_c(D_c/L)T^3\left[\frac{1}{3}-\frac{z_n}{T}\left(1-\frac{z_n}{T}\right)\right], \tag{40}$$

$$k=2\mu_c(LT/D_c)+\pi^2\sigma_c(D_c/L)T, \tag{41}$$

$$m=\rho LTD_c. \tag{42}$$

*Three-mass model (cover):*

$$I_c=\rho LTD_cT^2\left[\frac{1}{3}-\frac{z_n}{T}\left(1-\frac{z_n}{T}\right)\right], \tag{43}$$

$$k_1=2\mu_c(LT/D_c)z_n/T+\pi^2\sigma_c(D_c/L)z_n, \tag{44}$$

$$k_2=2\mu_c(LT/D_c)(1-z_n/T)+\pi^2\sigma_c(D_c/L)\times T(1-z_n/T), \tag{45}$$

$$k_c=\left\{\frac{1}{2}\mu_c(LD_c/T)\left[\frac{1}{3}-\frac{z_n}{T}\left(1-\frac{z_n}{T}\right)\right]^{-1}-2\mu_c(LT/D_c)\right\}\frac{z_n}{T}\left(1-\frac{z_n}{T}\right), \tag{46}$$

$$m_1=\rho LTD_cz_n/T, \tag{47}$$

$$m_2=\rho LTD_c(1-z_n/T). \tag{48}$$

*Both models (body):*

$$K=2\mu_bLT/D_b+\pi^2\sigma_b(D_b/L)T, \tag{49}$$

$$M=\rho LTD_b. \tag{50}$$

Note that for this nonisotropic tissue, all stiffnesses now depend on all vocal fold dimensions. It is no longer a simple matter to adjust shear or compression stiffness by vocal fold geometry. The anatomical resting depths of the layers of vocal fold tissue are gleaned from Hirano (1975):

$D_{\text{muc}}=$ depth of mucosa
$=$ epithelium + superficial layer
$=0.2$ cm in males (0.15 cm in females),

$D_{\text{lig}}=$ depth of ligament
$=$ intermediate + deep layer
$=0.2$ cm in males (0.15 cm in females),

$D_{\text{mus}}=$ depth of TA muscle (thyrovocalic portion)
$=0.4$ cm in males (0.3 cm in females).

According to Hirano (1975), the body and the cover share the depth of the ligament. The medial half, known as the intermediate layer of the lamina propria, is assigned to the cover, whereas the lateral half, known as the deep layer of the lamina propria, is assigned to the body. The fiber stress in the body is then made up of both muscle stress and ligament stress. But stresses do not add in parallel layers; rather, forces do. Hence, we convert the stresses to forces by multiplying by cross-sectional areas, or (since thickness is common) by the respective depths,

$$\sigma_b=[0.5\sigma_{\text{lig}}D_{\text{lig}}+\sigma_{\text{mus}}D_{\text{mus}}]/D_b, \tag{51}$$

where $\sigma_{\text{lig}}$ is the ligament stress and $\sigma_{\text{mus}}$ is the muscle stress. Likewise, for the cover,

$$\sigma_c=[\sigma_{\text{muc}}D_{\text{muc}}+0.5\sigma_{\text{lig}}D_{\text{lig}}]/D_c, \tag{52}$$

where $\sigma_{\text{muc}}$ is the mucosa stress.

The muscle stress has an active and a passive component (Alipour-Haghighi *et al.*, 1989)

$$\sigma_{\text{mus}}=a_{\text{TA}}\sigma_{\text{am}}\,\text{Max}[0,1-b(\epsilon-\epsilon_m)^2]+\sigma_p, \tag{53}$$

where $\sigma_{\text{am}}$ is the maximum active stress in the TA muscle fibers, $a_{\text{TA}}$ is the muscle activity (ranging from 0 to 1), and $\sigma_p$ is the passive stress. Note that the active stress varies with vocal fold strain $\epsilon$, falling off quadratically on both sides of an optimum sarcomere strain $\epsilon_m$, with $b$ being an empirically determined constant for a given muscle. The constants are given in Table I.

The cover has only a passive stress. This passive stress has been modeled with a combination of a linear and an exponential function and matched to vocal fold stress–strain curves (Alipour and Titze, 1991; Min *et al.*, 1995). The form of this function applies also to the passive stress of the body (muscle tissue and ligament tissue) and is written for all tissue types as

$$\sigma_p=\begin{cases}0 & \text{for } \epsilon<\epsilon_1,\\ -\dfrac{\sigma_0}{\epsilon_1}(\epsilon-\epsilon_1) & \text{for } \epsilon_1\leqslant\epsilon\leqslant\epsilon_2,\\ -\dfrac{\sigma_0}{\epsilon_1}(\epsilon-\epsilon_1)+\sigma_2[e^{C(\epsilon-\epsilon_2)}-C(\epsilon-\epsilon_2)-1] & \text{for } \epsilon>\epsilon_2.\end{cases} \tag{54}$$

TABLE I. Numerical constants used in Eqs. (53) and (54) to generate stress-strain curves for the cover, ligament, and muscle layers.

| Layer | $\epsilon_1$ | $\epsilon_2$ | $\sigma_0$ (kPa) | $\sigma_2$ (kPa) | $C$ | $\sigma_m$ (kPa) | $\epsilon_m$ | $b$ |
|---|---|---|---|---|---|---|---|---|
| mucosa | −0.5 | 0.35 | 0.5 | 30.0 | 4.4 | ⋯ | ⋯ | ⋯ |
| ligament | −0.5 | −0.00 | 0.4 | 1.393 | 17.0 | ⋯ | ⋯ | ⋯ |
| TA muscle | −0.5 | −0.05 | 1.0 | 1.50 | 6.5 | 105 | 0.4 | 1.07 |

In Eq. (54), $\sigma_o$ is the stress when $\epsilon=0$, $\epsilon_1$ is the strain where the linear portion goes to zero, $\sigma_2$ is a scale factor for the exponential portion, and $\epsilon_2$ is the strain where the exponential portion begins. These constants have been fitted individually to each stress–strain curve and are reported in Table I.

This concludes the physics of the models for natural (undamped and undriven) oscillation. For damped oscillation, it is typical to assign a damping ratio of 0.1–0.2 to each mass (Kaneko *et al.*, 1981; Chan and Titze, 1999). But for self-sustained oscillation, the low-dimensional models require a higher degree of damping for the less dominant modes. This broadens their frequency spectrum and allows for better entrainment to the dominant mode, which is usually the compressional mode of the body. This was already discovered by Ishizaka and Flanagan (1972) with their two-mass model. They made the compressional mode of the lower mass dominant, assigning it a damping ratio of 0.1. The upper mass was given a damping ratio of 0.6 for better entrainment. We will also use this value for the upper mass, while keeping the lower mass and the body mass at a damping ratio of 0.1.

## IV. DEVELOPMENT OF RULES FOR MUSCLE CONTROL

In this section we develop rules for controlling the geometric and elastic parameters of the body-cover model by muscle activation. These rules take the place of the physics of deformable bodies for vocal fold posturing (adducting and elongating). To reduce the number of control parameters, only the cricothyroid activity ($a_{\mathrm{CT}}$), the thyroarytenoid activity ($a_{\mathrm{TA}}$), and the lateral cricoarytenoid activity ($a_{\mathrm{LC}}$) will be considered. The effect of the interarytenoid muscle is neglected and the effect of the posterior cricoarytenoid muscle is included by allowing $a_{\mathrm{LC}}$ to become negative. Some of the rules are not yet in their final stage of development, but are quite functional at this point. We begin with the elongation rule.

### A. Elongation rule

Experimentation with excised larynges and *in vivo* animal preparations (Titze *et al.*, 1988, 1997) has shown that vocal fold elongation can be expressed in the form

$$\epsilon = G(Ra_{\mathrm{CT}} - a_{\mathrm{TA}}) - Ha_{\mathrm{LC}}, \tag{55}$$

where $\epsilon$ is the longitudinal vocal fold strain (elongation divided by the cadaveric rest length), $a_{\mathrm{CT}}$ is the normalized cricothyroid muscle activity (ranging from 0.0 to 1.0), $a_{\mathrm{TA}}$ is the normalized thyroarytenoid muscle activity (same range), and $a_{\mathrm{LC}}$ is the normalized lateral cricoarytenoid muscle activity (same range). The empirical constants in the equation are the gain of elongation $G$, the torque ratio $R$, and the adductory strain factor $H$. This rule has been modified from a previous rule (Titze *et al.*, 1988) to include the adductory strain $Ha_{\mathrm{LC}}$ that occurs for prephonatory posturing. This inclusion left the nature of the equation the same, but changes the coefficients slightly. For this study, we are letting $G=0.2$, $R=3.0$, and $H=0.2$. The previous rule was for canines, whereas the current version is intended for humans, for which the range of $\epsilon$ must be higher to achieve a larger pitch range. Thus, $G$ was increased from 0.1 to 0.2 for humans. With this gain, the maximum elongation is 60% when $a_{\mathrm{CT}}=1.0$ and $a_{\mathrm{TA}}=a_{\mathrm{LC}}=0$. This replaces the maximumal superior nerve stimulation condition in the Titze *et al.* (1997) study, for which the canine vocal folds elongated a maximum of 45%. The maximum shortening in Eq. (55) occurs for $a_{\mathrm{CT}}=0$ and $a_{\mathrm{TA}}=a_{\mathrm{LC}}=1.0$. For this case, the rule gives −40%, as compared to the measured canine value of −17% under maximal recurrent nerve stimulation. With full contraction of all muscles, the rule gives 20% elongation as compared to the measured value of 26% for canines.

We cannot expect phonation to be realizeable over the full range of elongation. Some of the extreme muscle contractions stiffen the vocal folds too much or shut off the glottis. Nishizawa *et al.* (1988) observed an approximate 2:1 ratio between the shortest and the longest vocal folds when subjects phonated over wide pitch ranges. In the rule given above, the range of $\epsilon$ is −30% to 50% when $a_{\mathrm{LC}}$ is chosen to be 0.5. This corresponds to a length change of $0.7L_o$ to $1.5L_o$, where $L_o$ is the resting length, a range quite similar to that reported by Nishizawa *et al.*

With the above rule, the vocal fold length can be written as

$$L = L_o(1+\epsilon) \tag{56}$$

$$= L_o[1 + G(Ra_{\mathrm{CT}} - a_{\mathrm{TA}}) - Ha_{\mathrm{LC}}], \tag{57}$$

where $L_o$ is 1.6 cm in males and 1.0 cm in females.

### B. Nodal point rule

When the TA muscle contracts, the bottom edge adducts more than the top edge, reducing the convergence angle (see convergence rule below). Concurrently, the nodal point $z_n$ for the shear mode effectively moves up on the medial surface, suggesting that there is greater vibrational amplitude at the bottom relative to the top. Empirically, this is related to the point of mucosal upheaval (Yumoto *et al.*, 1993). We propose the rule

$$z_n = (1 + a_{\mathrm{TA}})T/3. \tag{58}$$

With this rule, the nodal point is one-third from the bottom for falsetto register (thin vocal folds and greatest amplitude at the top) and one-third from the top in modal register (thick vocal folds with greater amplitude at the bottom). This rule is one of the weaker ones and will probably undergo modifications when more data become available.

### C. Thickness and depth rules

In a purely passive sense, vocal fold thickness increases with vocal fold shortening. The Poisson ratio of continuous elastic media determines this increase. For an incompressible isotropic medium, the Poisson ratio is 0.5, but since medial-lateral expansion or contraction is constrained by the arytenoid and thyroid cartilage boundaries, most (or all) of the length change is absorbed by thickness change. Thus, our thickness rule is

$$T = \frac{T_o}{1+0.8\epsilon}, \tag{59}$$

where $T_o$ is the vibrating thickness at resting length. Since the low-dimensional models do not have a medial surface curvature, we limit $T_o$ to be 0.30 cm for males and 0.20 cm for females, as discussed earlier with regard to Eq. (37).

The depth rules are then as follows:

$$D_b = \frac{a_{\mathrm{TA}} D_{\mathrm{mus}} + 0.5 D_{\mathrm{lig}}}{1+0.2\epsilon}, \tag{60}$$

$$D_c = \frac{D_{\mathrm{muc}} + 0.5 D_{\mathrm{lig}}}{1+0.2\epsilon}, \tag{61}$$

where the $0.2\epsilon$ factor in the denominator represents the complement to the $0.8\epsilon$ factor for thickness. In the numerator, the terms represent portions of the mucosa, ligament, and muscle. For $a_{\mathrm{TA}}=0$, the deep layer of the lamina propria (half of the ligament) is the sole depth of the body; whereas, for $a_{\mathrm{TA}}=1$, the entire depth of the muscle is added to the body depth.

### D. Adduction rule

The following adduction rule for the glottal half-width $\xi_{02}$ at the vocal fold processes (Fig. 1) is chosen on the basis of fiberscopic measurements:

$$\xi_{02} = 0.25 L_o (1 - 2.0 a_{\mathrm{LC}}), \tag{62}$$

where $a_{\mathrm{LC}}$ is the activation of the lateral cricoarytenoid muscle. This rule anchors the "just touching" ($\xi_{02}=0$) position at $a_{\mathrm{LC}}=0.5$. For $a_{\mathrm{LC}}>0.5$ the vocal processes are pressed together (actually overlapped). For $a_{\mathrm{LC}}<0.5$, the vocal processes are separated. We allow $a_{\mathrm{LC}}$ to include the range 0 to $-1$ for *abduction* of the vocal processes, thereby simulating the action of the posterior cricoarytenoid muscle as an antagonist in this range.

Data by Scherer (1995) suggest that oscillation is obtained over about 10% of the range of motion of the vocal process. This range of motion was expressed by Scherer as a vocal process gap to length ratio ($2\xi_{02}/L_o$). Scherer's data were obtained with fiberscopic measurements on human subjects. A range of 0–1.5 for $2\xi_{02}/L_o$ is achieved in our rule when $a_{\mathrm{LC}}$ ranges from 0.5 to $-1$. This follows Scherer's claim that the maximum glottal gap at the vocal processes is about 50% greater than the vocal fold length for rapid inhalation.

The cadaveric (rest) position occurs for $a_{\mathrm{LC}}=0$, which yields a vocal process gap to length ratio of 0.5 in our rule. The ratio reported by Scherer for quiet respiration was 0.68, which may not represent exactly zero muscle activation. In our rule, Scherer's ratio of 0.68 would be slightly abductory activation ($a_{\mathrm{LC}}=-0.18$). For phonation threshold, Scherer claims a process gap to a length ratio of 0.17, which by our rule would occur for $a_{\mathrm{LC}}=0.33$ and would be 11% of the range of 0 to 1.5.

### E. Convergence rule

Glottal convergence and medial surface bulging are, to a large extent, governed by activation of the thyroarytenoid muscle (Hirano, 1975). The critical issue for self-sustained oscillation is that a portion of the medial surface of the vocal folds must always be nearly vertical to produce a section of the glottis that is nearly rectangular (Chan *et al.*, 1997). This nearly rectangular glottal section can be achieved over a large portion of the human vocal fold thickness in modal register, since the medial surface has convex curvature (bottom to top), but only near the top of the fold in falsetto register. It would require at least three masses to be stacked vertically in a model to approximate this quadratic surface and thereby obtain a partial rectangular glottis. With the low-dimensional models under consideration here, three vertically stacked masses is not an option, which severely restricts the range of convergence under which the models can operate. With reference to Fig. 1, we propose the following rule for convergence:

$$\xi_c = \xi_{01} - \xi_{02} = T(0.05 - 0.15 a_{\mathrm{TA}}). \tag{63}$$

With this rule, the range of $\tan\theta_0 = \xi_c/T$ is from 0.05 to $-0.1$, which produces shapes from slightly convergent ($+3°$ at $a_{\mathrm{TA}}=0$) to moderately divergent ($-6°$ at $a_{\mathrm{TA}}=1$). But even with this restricted range of convergence and divergence, not all of these shapes produce self-sustained oscillation, as we will show. A rectangular glottis, which was shown to be ideal for phonation in a physical model (Chan *et al.*, 1997), is obtained for $a_{\mathrm{TA}}=0.33$. We will show that the best configu-

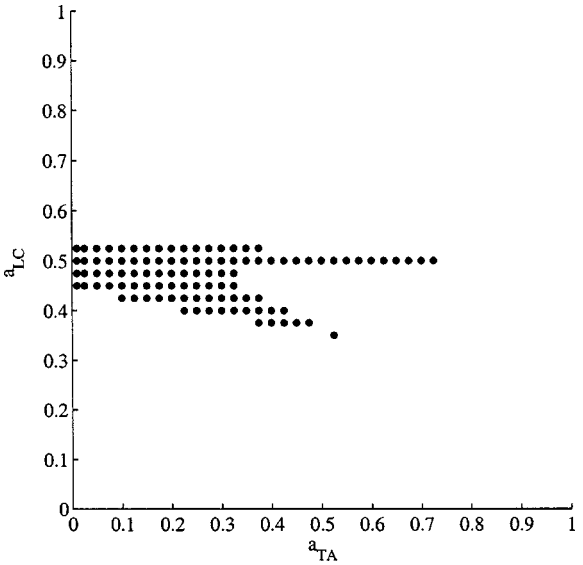


FIG. 2. Muscle activation plot (MAP) for lateral cricoarytenoid activity ($a_{\mathrm{LC}}$) versus thryoarytenoid activity ($a_{\mathrm{TA}}$). Data points show region of self-sustained oscillation with the convergence rule [Eq. (63)]. Cricothyroid activity ($a_{\mathrm{CT}}$) was fixed at 0.2 and lung pressure was fixed at 0.8 kPa.

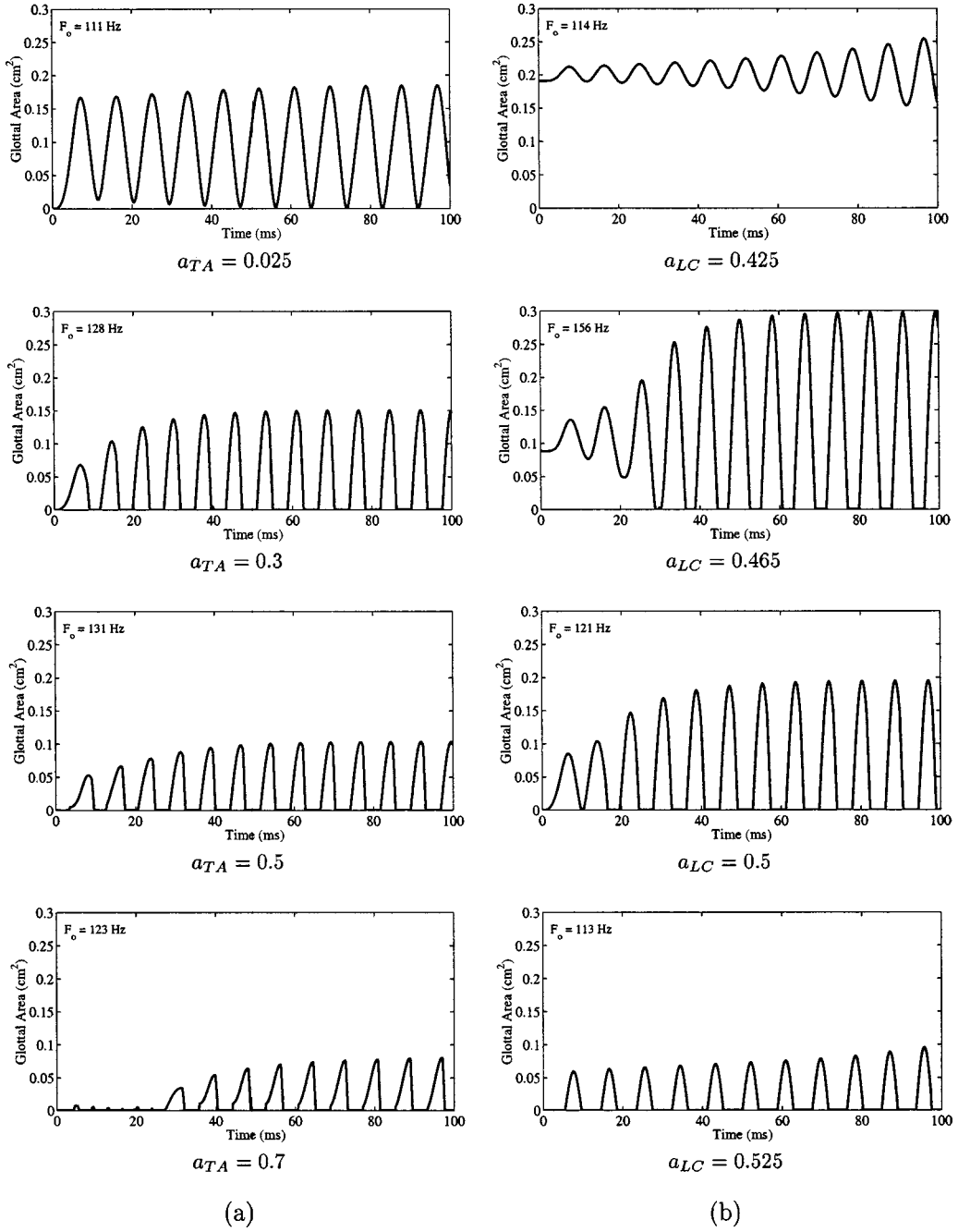


FIG. 3. Glottal area waveforms for selected sections through the adductory MAP of Fig. 2. (a) $a_{\mathrm{LC}}=0.5$ and (b) $a_{\mathrm{TA}}=0.25$. In both cases, $a_{\mathrm{CT}}$ was fixed at 0.2 and lung pressure was fixed at 0.8 kPa.

ration is an almost negligibly small convergence ($\theta \approx 0.0001$), which allows for complete adduction at the top ($\xi_{02}=0$) while full subglottal pressure is applied to the vocal folds when the bottom is barely abducted ($\xi_{01}=0.0005\,\mathrm{cm}$). We shall refer to this as the ''nearly rectangular'' case.

## V. RESULTS

Figure 2 shows the region of oscillation of the bar-plate model in an adductory muscle activation plot (adductory MAP). The figure was created by performing separate 200 ms simulations for multiple pairs of TA and LCA activities. TA muscle activity is plotted horizontally, LCA activity is plotted vertically, and each dot denotes a pair of activities at which oscillation was sustained. Lung pressure was constant at 0.8 kPa (approximately 8 cm $H_2O$), $a_{\mathrm{CT}}$ was held constant at 0.2, and the convergence rule was used [Eq. (63)]. Existence of self-sustained phonation at each activation pair was determined by applying a zero-crossing detector to the last 100 ms of the simulated glottal area signal. Note that phonation is restricted to a small region of this MAP, as was expected from the results of Scherer (1995), on which our adduction rule was based. Oscillation occurs approximately along a constant horizontal line ($a_{\mathrm{LC}}=0.5$), but there appears to be a second (downward sloping) path for which an increase in $a_{\mathrm{TA}}$ must be counterbalanced with a slight decrease in $a_{\mathrm{LC}}$.

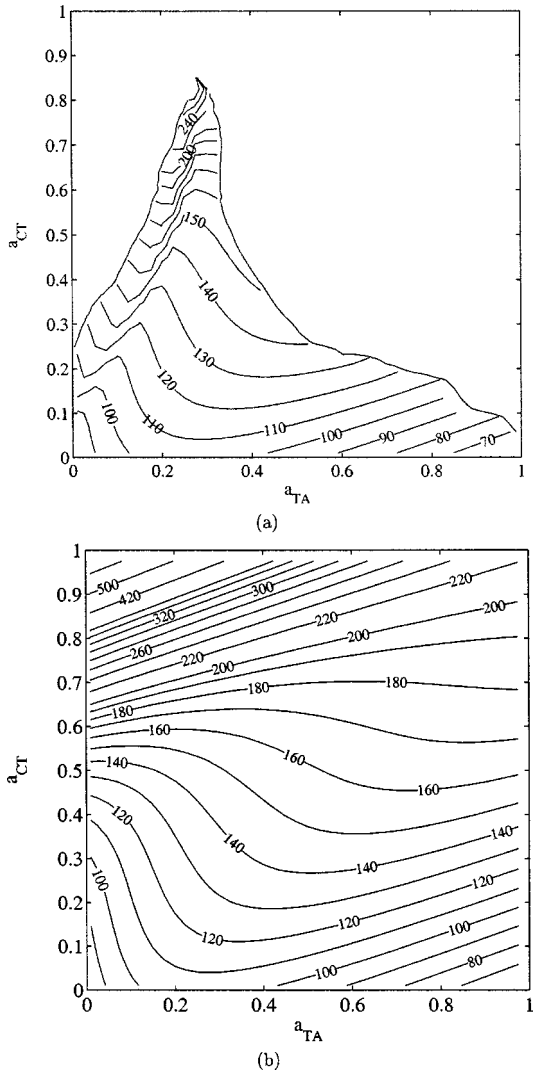


FIG. 4. Muscle activation plot (MAP) for cricothyroid activity ($a_{CT}$) versus thyroarytenoid activity ($a_{TA}$) with $F_o$ contour lines. (a) The convergence rule [Eq. (63)] and (b) ''nearly rectangular'' convergence.

Figure 3 shows glottal area waveforms associated with the adductory MAP of Fig. 2. Part (a) shows waveforms for a *horizontal* section through the MAP at $a_{LC}=0.5$. Thyroarytenoid activity ($a_{TA}$) increases from top to bottom. Note that the glottal area is nearly sinusoidal at $a_{TA}=0.025$, but increases in both skewing and glottal closure when $a_{TA}$ is increased to 0.7. Voice onset is delayed with $a_{TA}=0.7$. Note also that the amplitude of the glottal area decreases with $a_{TA}$, which is expected with greater adduction at the bottom of the fold and increased mass of the body (*vis-a-vis* our rules).

Figure 3(b) shows waveforms for a *vertical* section through the adductor MAP, namely for $a_{TA}=0.25$. Lateral cricoarytenoid activity ($a_{LC}$) now increases from 0.425 at the top to 0.525 at the bottom. Note that there is first an increase in glottal area amplitude (from very slow voice onset to rapid onset with large peak-to-peak variations), followed by a decrease in glottal area amplitude. This supports the notion that there is an optimal adduction for maximal power transfer in the ''pressed voice'' to ''breathy voice'' continuum (Titze, 2002).

Glottal airflow waveforms are not shown here because they are not remarkably different from the area waveforms. We have deliberately decoupled the vocal tracts (subglottal and supraglottal) for this investigation because its inclusion would have complicated the parameter set. Hence, for this decoupled vocal tract case, all of the glottal airflow waveforms looked similar to the area waveforms, with the typically larger skewing quotient of airflow (due to vocal tract inertance) being absent.

Figure 4 is a muscle activation plot (MAP) for elongating and tensing the vocal folds, showing $a_{CT}$ on the vertical axis and $a_{TA}$ on the horizontal axis. Contour lines are for constant $F_o$ in Hz. Part (a) is for the convergence rule [Eq. (63)] while part (b) is for the ''nearly rectangular'' case. Note that the ''nearly rectangular'' configuration (part b) produces oscillation over the entire MAP (all values of $a_{CT}$ and $a_{TA}$) whereas the rule-based configuration (part a) is severely restricted in the upper quadrants. In particular, for large values of $a_{CT}$ (high frequencies), only a small range of values of $a_{TA}$ (between 0.2 and 0.4) produces oscillation. It seems to be important to keep the glottis slightly convergent (below $a_{TA}=0.33$). This generates a strong asymmetry in the aerodynamic driving forces (a push-pull mechanism) for outward versus inward movement of the vocal folds (Titze, 1994, Chap. 4).

An important feature of these MAPs is the downward bending of the contour lines in the lower left quadrant, where most speech occurs. Because of this downward bending, $F_o$ can be raised by increasing either $a_{CT}$ or $a_{TA}$. In other quadrants (especially the upper left), an increase in $a_{TA}$ will generally cause a decrease in $F_o$. (For a thorough review of this $F_o$ control mechanism see Titze, 1994, Chap. 8.)

Figure 5 shows glottal area waveforms for vertical and horizontal sections through the MAP of Fig. 4(b). On the left [Fig. 5(a)] are waveforms for a vertical section (with $a_{TA}$ constant at 0.25 and $a_{CT}$ ranging from 0.05 to 0.9); on the right [Fig. 5(b)] are waveforms for a horizontal section (with $a_{CT}$ constant at 0.25 and $a_{TA}$ ranging from 0.05 to 0.9). Adduction is held constant throughout at $a_{LC}=0.5$ and convergence is the ''nearly rectangular'' case. Note that the effect of increasing $a_{CT}$ (left side, top to bottom) is to increase $F_o$ slightly at first (for values of $a_{CT}<0.5$) but more dramatically later (for values of $a_{CT}>0.5$). The amplitude of vibration decreases with increasing $a_{CT}$ and there is a slight decrease of adduction with this amplitude change. The effect of increasing $a_{TA}$ (right side, top to bottom) is to obtain a small increase in $F_o$ at first, followed by a small decrease (when $a_{TA}>0.5$). This is a direct result of the curvature of the constant $F_o$ lines in Fig. 4. The amplitude also decreases with increasing $a_{TA}$, and there is an increase in waveform skewing (seen best in the bottom right plot).

Figure 6 shows tensor MAPs with mode frequencies $F_1$, $F_2$, and $F_3$ as contour parameters. Note that for mode 1, the principal compressional mode, the MAP exhibits downward sloping $F_1$ curves in the lower left quadrant. In fact, the MAP is strikingly similar to the self-oscillation MAP of Fig. 4(b), suggesting that $F_o$ is controlled by $F_1$, the compressional mode in the body. Again, the downward sloping curves allow for maximal increase in frequency with $a_{TA}$,

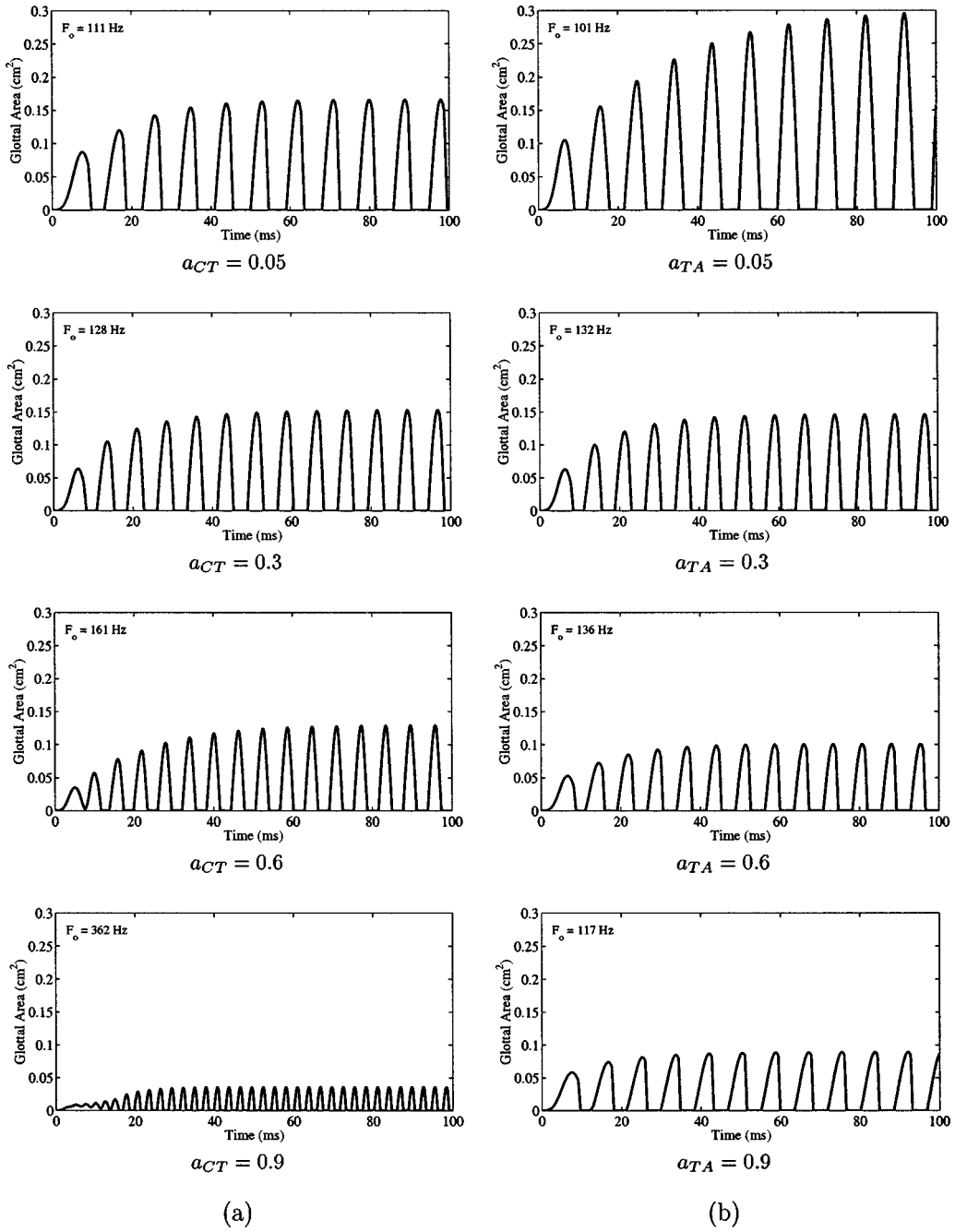


FIG. 5. Glottal area waveforms for selected sections through the tensor MAP of Fig. 4(b). (a) $a_{\mathrm{TA}}=0.25$ and (b) $a_{\mathrm{CT}}=0.25$. In both cases, $a_{\mathrm{LC}}$ was fixed at 0.5 and lung pressure was fixed at 0.8 kPa.

since frequency increase is always perpendicular to the contour lines. Downward sloping contour lines for $F_o$ were shown to exist in human subjects (Titze *et al.*, 1989). For large $a_{\mathrm{CT}}$ [top half of Fig. 6(a)], maximum $F_1$ increase occurs primarily in the direction of increasing $a_{\mathrm{CT}}$ (upward), especially in the upper left quadrant.

The shear mode [mode 2, Fig. 6(b)] and the higher compressional mode [mode 3, Fig. 6(c)] show monotonic frequency increases with $a_{\mathrm{CT}}$ and monotonic decreases with $a_{\mathrm{TA}}$. These modes are generally entrained to mode 1 in self-sustained oscillation as discussed previously. Note that $F_2$ is generally about twice $F_1$ for the same muscle activities, providing a likely 2:1 entrainment. Mode 3 is likely to be entrained in a 3:1 ratio to mode 1.

Figure 7 shows how the stiffnesses $k_1$, $k_2$, $k_c$, and $K$, vary with the muscle activities. Note that $K$ in Fig. 7(d) (the body stiffness) is dominant in controlling the mode 1 frequency, given that the contour lines are most similar to those of the natural frequency of mode 1, except in the lower right corner. The cover stiffnesses $k_1$ and $k_2$ increase monotonically with $a_{\mathrm{CT}}$ and decrease monotonically with $a_{\mathrm{TA}}$. The coupling stiffness $k_c$ first decreases with $a_{\mathrm{TA}}$ and then increases again. In particular, $k_c$ increases for $a_{\mathrm{TA}}<0.5$ and decreases for $a_{\mathrm{TA}}>0.5$. This is a consequence of the nodal rule [Eq. (58)], which gives the torsional stiffness in the cover the largest value when the nodal point is at the center.

In Fig. 8, we show the tensor MAPs once again, but this time the contour parameter is tissue mass. Figure 8(a) is for

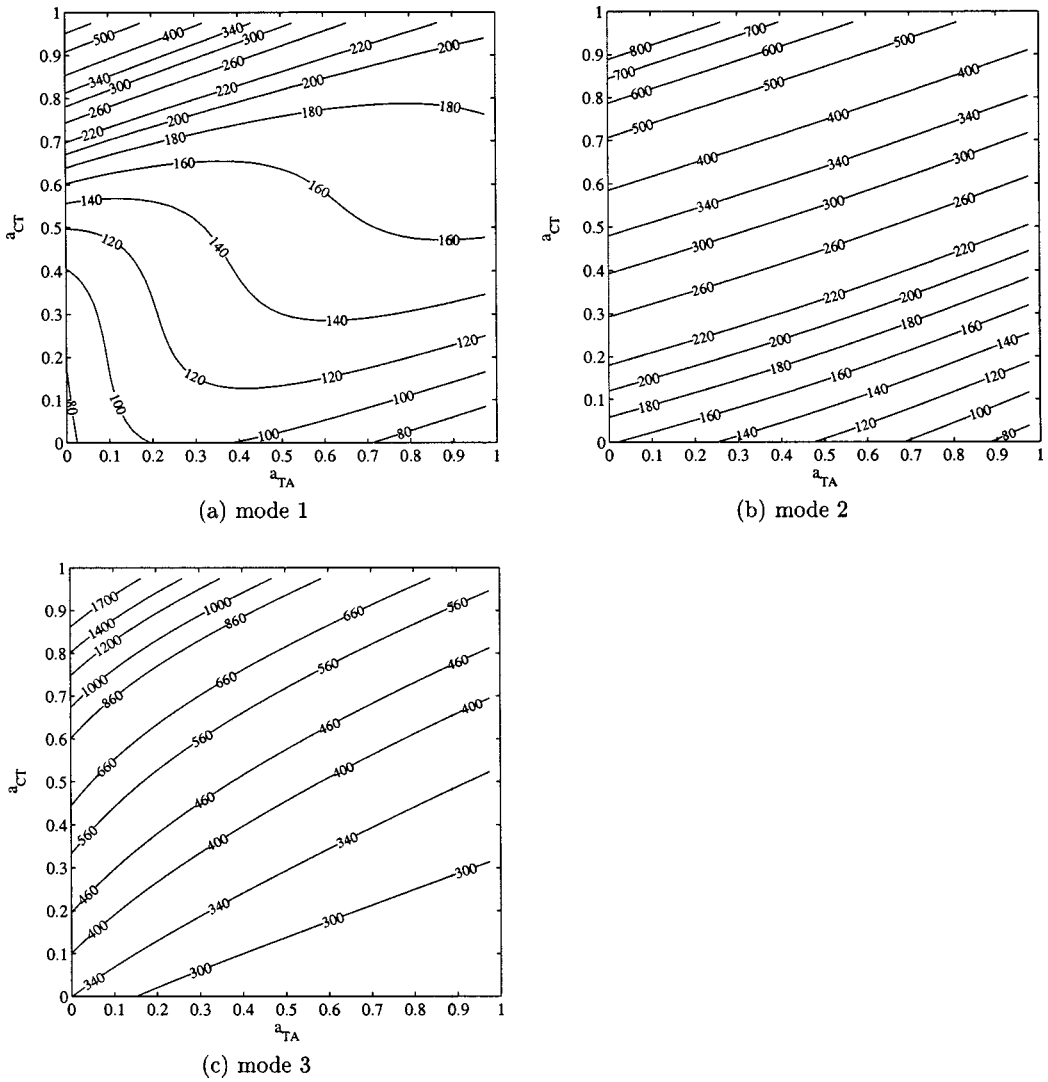


FIG. 6. Muscle activation plots (MAPs) for cricothyroid activation ($a_{CT}$) versus thyroarytenoid activation ($a_{TA}$) with normal mode frequencies as contour parameter. (a) Mode 1, the principal compressional mode, (b) mode 2, the shear mode, and (c) mode 3, the higher compressional mode. These plots are based on the rules developed in this paper.

the lower cover mass $m_1$, Fig. 8(b) is for the upper cover mass $m_2$, and Fig. 8(c) is for the body mass $M$. Note that all masses increase monotonically with $a_{TA}$ and are nearly unaffected by $a_{CT}$ as a result of our rules.

## VI. CONCLUSIONS

Low-dimensional models of the vocal folds can be made to oscillate in a semi-realistic way with muscle activations, but rules are necessary to capture the covariation between parameters. In particular, the medial surface of the vocal folds, which is quantized by only two vertical compartments, must be nearly rectangular for self-sustained oscillation to occur over a wide region of muscle activities.

In order to incorporate a fibrous (stringlike) elastic restoring force as well as a nonfibrous (gellike) restoring forces, the spring constants can be constituted of multiple terms that incorporate measurable elastic moduli and fiber tensions. Both active and passive muscle properties can be incorporated. Co-contraction between the cricothyroid and thyroarytenoid muscles produce oscillation regions (and fundamental frequency contours) that are quite comparable to those that have been measured. The overall frequency range is also comparable to what is expected for humans (about 100–500 Hz). A deliberate omission in this work has been the acoustic loading of the vocal tract (both subglottal and supraglottal). It is well known that the oscillation regions of any interactive model are affected by acoustic loading, but this complexity was not warranted for this study because the focus was on vocal fold tissue characteristics.

It is conceivable that improvements could be made by letting the depths of the muscle tissue be a function of lung pressure. Such a rule is presently being investigated, but little data are available for vibration depth as a function of driving pressure. At this point, the control of depth is by intrinsic muscle activation only.

One of the most severe restrictions of low-dimensional models is the exclusion of vertical movement of the tissue. Much more variability in the medial shaping of the glottis (e.g., more convergence and divergence) is possible if the tissue is simultaneously driven upward and outward, forming elliptical trajectories. But that would double the degrees of freedom and would minimize the interpretive power that

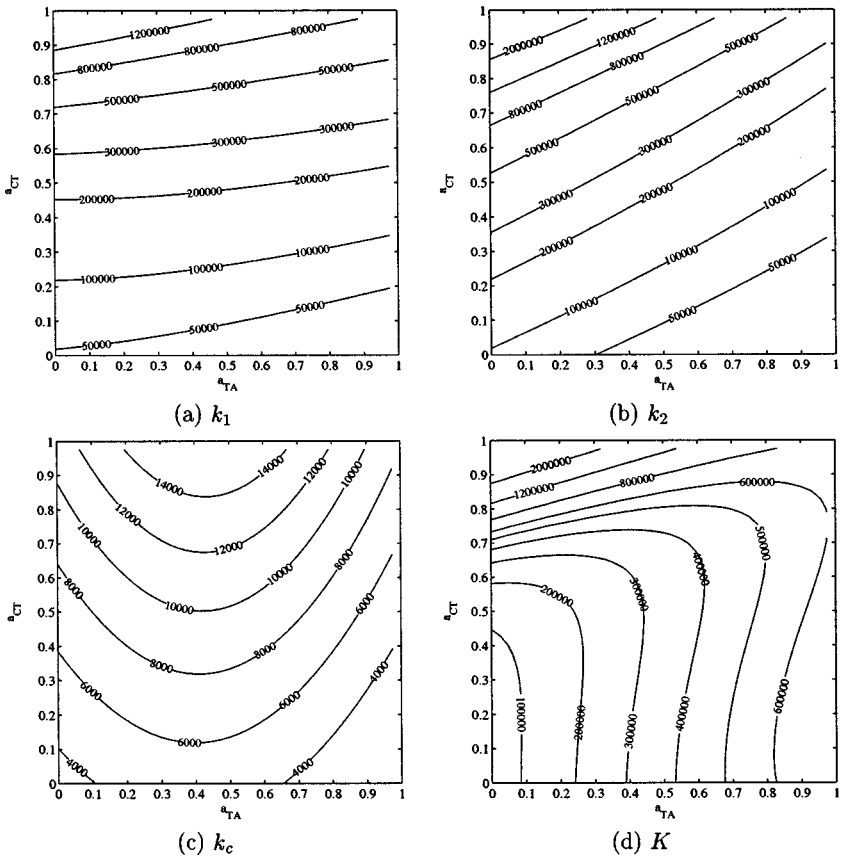


FIG. 7. Muscle activation plots (MAPs) for cricothyroid activation ($a_{CT}$) versus thyroarytenoid activation ($a_{TA}$) with the lumped-element spring constants as contour parameters. (a) Lower spring of cover, (b) upper spring of cover, (c) coupling spring of cover, and (d) spring of body.

nonlinear dynamics can offer. This paper has focused on low-dimensional vocal fold models (three degrees of freedom) and its rules for physiologic control. It cannot be overstated that pushing these rules, and the general use of low-dimensional models, much beyond this point may be counter-productive. Specifically, to investigate many aspects of vocal quality and for modeling pathology, we recommend higher-dimensional models and fewer rules.

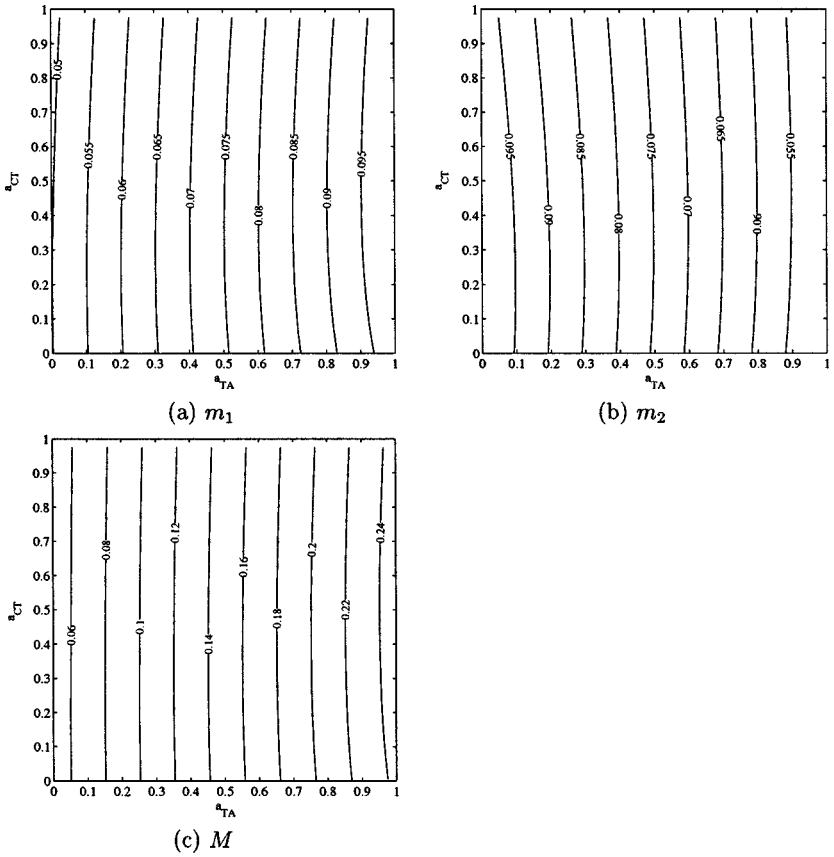


FIG. 8. Muscle activation plot (MAP) for cricothyroid activity $a_{CT}$ versus thyroarytenoid activity $a_{TA}$ with lumped element masses as contour parameters. (a) Lower mass of cover, (b) upper mass of cover, and (c) mass of body.

## ACKNOWLEDGMENTS

This work was supported by Grant No. R01 DC04347 from the National Institute on Deafness and Other Communication Disorders. The authors also thank Sarah Klemuk for assistance in manuscript preparation.

Alipour-Haghighi, F., and Titze, I. R. (**1983**). ''Simulation of particle trajectories of vocal fold tissue during phonation,'' in *Vocal Fold Physiology: Biomechanics, Acoustics and Phonatory Control*, edited by I. Titze and R. Scherer, Denver Center for the Performing Arts, pp. 183–190.

Alipour-Haghighi, F., and Titze, I. R. (**1991**). ''Elastic models of vocal fold tissues,'' J. Acoust. Soc. Am. **90**, 1326–1331.

Alipour-Haghighi, F., and Titze, I. R. (**1996**). ''Combined simulation of two-dimensional air and vocal fold vibration,'' in *Vocal Fold Physiology: Controlling Complexity and Chaos*, edited by P. Davis and N. Fletcher (Singular, San Diego), pp. 17–29.

Alipour-Haghighi, F., Titze, I. R., and Perlman, A. L. (**1989**). ''Tetanic contraction in vocal fold muscle,'' J. Speech Hear. Res. **32**, 226–231.

Baer, T. (**1975**). ''Investigation of phonation using excised larynges,'' doctoral dissertation, Massachusetts Institute of Technology, Cambridge, MA.

Berry, D. A., and Titze, I. R. (**1996**). ''Normal modes in a continuum model of vocal fold tissues,'' J. Acoust. Soc. Am. **105**, 3345–3354.

Berry, D. A., Moon, J. B., and Kuehn, D. P. (**1999**). ''A finite element model of the soft palate,'' Cleft Palate Craniofac J. **36**(3), 217–223.

Chan, R., and Titze, I. R. (**1997**). ''Dynamic shear modulus of vocal fold tissues and phonosurgical biomaterials,'' J. Acoust. Soc. Am. **101**, 3179(A).

Chan, R., and Titze, I. R. (**1999**). ''Viscoelastic shear properties of human vocal fold mucosa: Measurement methodology and empirical results,'' J. Acoust. Soc. Am. **106**, 2008–2012.

Chan, R., Titze, I. R., and Titze, M. (**1997**). ''Further studies of phonation threshold pressure in a physical model of the vocal fold mucosa,'' J. Acoust. Soc. Am. **101**, 3722–3727.

Flanagan, J. L., and Landgraf, L. L. (**1968**). ''Self-oscillating source for vocal-tract synthesis,'' IEEE Trans. Audio Electroacoust. **AU-16**(1), 57–64.

Fung, Y. C. (**1993**). *Biomechanics: Mechanical Properties of Living Tissue*, 2nd ed. (Springer Verlag, New York).

Hirano, M. (**1975**). ''Phonosurgery: Basic and clinical investigations,'' in 78th annual convention of the Oto-Rhino-Laryngological Society of Japan, 78th annual convention of the Oto-Rhino-Laryngological Society of Japan.

Ishizaka, K., and Flanagan, J. L. (**1972**). ''Synthesis of voiced sounds from a two-mass model of the vocal cords,'' Bell Syst. Tech. J. **51**(6), 1233–1268.

Kaneko, T., Uchida, K., Suzuki, H., Komatsu, K., Kanesaka, T., Kobayashi, N., and Naito, J. (**1981**). ''Mechanical properties of the vocal fold: Measurements *in vivo*,'' in *Vocal Fold Physiology*, edited by K. N. Stevens and M. Hirano (Tokyo U.P., Tokyo), pp. 365–376.

Liljencrants, J. (**1991**). ''A translating and rotating mass model of the vocal folds,'' STL Quarterly Progress and Status Report, 1, Speech Transmission Laboratory (Royal Institute of Technology (KTH), Stockholm, Sweden), pp. 1–18.

Min, Y., Titze, I. R., and Alipour-Haghighi, F. (**1995**). ''Stress-strain response of the human vocal ligament,'' Ann. Otol. Rhinol. Laryngol. **104**(7), 563–569.

Nishizawa, N., Sawashima, M., and Yonemoto, K. (**1988**). ''Vocal fold length in vocal pitch change,'' in *Vocal Physiology: Voice Production, Mechanisms and Functions*, edited by O. Fujimura (Raven, New York), pp. 75–82.

Pelorson, X., Hirschberg, A., van Hassel, R., Wijnands, A., and Auregan, Y. (**1994**). ''Theoretical and experimental study of quasi-steady separation within the glottis during phonation. Application to a modified two-mass model,'' J. Acoust. Soc. Am. **96**, 3416–3431.

Scherer, R. (**1995**). ''Laryngeal function during phonation,'' in *Diagnosis and Treatment of Voice Disorders*, edited by J. Rubin, R. Sataloff, G. Korovin, and W. Gould (IGAKU-SHOIN, New York).

Story, B. H., and Titze, I. R. (**1995**). ''Voice simulation with a body cover model of the vocal folds,'' J. Acoust. Soc. Am. **97**, 1249–1260.

Titze, I. R. (**2002**). ''Regulating glottal air in phonation: application of the maximum power transfer theorem,'' J. Acoust. Soc. Am. **111**, 67–76.

Titze, I. R., and Strong, W. (**1975**). ''Normal modes in vocal cord tissues,'' J. Acoust. Soc. Am. **57**, 736–744.

Titze, I. R., and Talkin, D. T. (**1979**). ''A theoretical study of the effects of various laryngeal configurations on the acoustics of phonation,'' J. Acoust. Soc. Am. **66**, 60–74.

Titze, I. R., Jiang, J., and Druker, D. (**1988**). ''Preliminaries to the body-cover theory of pitch control,'' J. Voice **1**(4), 314–319.

Titze, I. R., Luschei, E. S., and Hirano, M. (**1989**). ''The role of the thyroarytenoid muscle in regulation of fundamental frequency,'' J. Voice **3**(3), 213–224.

Titze, I. R. (**1994**). *Principles of Voice Production* (Prentice–Hall, Englewood Cliffs, NJ).

Titze, I. R., Jiang, J. J., and Lin, E. (**1997**). ''The dynamics of length change in canine vocal folds,'' J. Voice **11**(3), 267–276.

Titze, I. R., Jiang, J. J., and Hsiao, T. Y. (**1993**). ''Measurement of mucosal wave propagation and vertical phase difference in vocal fold vibration,'' Ann. Otol. Rhinol. Laryngol. **102**(1), 58–63.

Wilhelms-Tricarico, R. (**1995**). ''Physiological modeling of speech production: Methods for modeling soft-tissue articulators,'' J. Acoust. Soc. Am. **97**, 3085–3098.

Yumoto, E., Katota, Y., and Kurokawa, H. (**1993**). ''Tracheal view of vocal fold vibration in excised canine larynxes,'' Arch. Otolaryngol. Head Neck Surg. **119**(1), 73–78.